ESTIMATING BODYWAVE ARRIVALS AND ATTENUATION FROM SEISMIC NOISE

Peter Gerstoft[1], Jian Zhang[1], and Steven R Taylor[2]

University of California, San Diego[1] and Rocky Mountain Geophysics, LLC [2]

Sponsored by the Air Force Research Laboratory

Award No. FA8718-07-C-0005
Proposal No. BAA07-70

ABSTRACT

This paper investigates the utility of computing Time-Domain Green's Functions (TDGF) to be used for estimating velocity and attenuation structure for the purposes of nuclear explosion monitoring over local and near-regional distances. We have focused on two topics:

Earth's background vibrations at frequencies below about 0.5 Hz have been attributed to ocean-wave energy coupling into the ground and propagating as surface waves and *P* waves (compressional waves deep within the Earth). However, the origin and nature of seismic noise on land at frequencies around 1 Hz has not yet been well studied. Using array beamforming, we analyze the seismic noise fields at two remote sites (Parkfield and Mojave Deserts) in California, for durations of one and six months respectively. We find that (1) the seismic background noise at about 0.6–2 Hz consists of a significant amount of continuous *P* waves originating offshore, and (2) the power of the *P*-wave noise is highly correlated with the offshore wind speed, demonstrating that these high-frequency *P* waves are excited by distant ocean winds.

We present a methodology to obtain frequency-dependent relative site amplification factors using ambient seismic noise. We treat a seismic network or array as a forced damped harmonic oscillator system where each station responds to a forcing function obtained from frequency-wavenumber beams of the ambient noise field. Taken over long time periods, each station responds to the forcing function showing a frequency-dependent resonance peak whose amplitude and spectral width depends upon the elastic and anelastic properties of the underlying medium. Our results are encouraging in that hard rock sites generally show narrower resonance peaks with reduced amplitudes relative to soft rock sites in sedimentary basins. There is also a tendency for spectral peaks to shift to higher frequencies and become more asymmetric as the site amplification increases. This could be due to small-strain nonlinearity for stations having high site amplification.

One exciting aspect of this research is that noise analysis methods have the potential to be very useful in improving body-wave tomography for Earth's structure, just as noise cross-correlation methods have recently proven successful in surface-wave tomography. A preliminary test examining teleseismic *P* waves recorded in southern California shows that similar arrival-time anomalies can be obtained both from direct *P* waves from a natural earthquake and *P*-wave noise generated by a large storm. In this case, the noise can be processed using waveform cross-correlation among different station pairs and optimal P relative arrival-time estimates can be computed using the same approach traditionally used to analyze earthquake arrival times.

OBJECTIVES

Our objective is to apply and extend the methodology of deriving TDGF for propagation between two receivers by cross-correlation of seismic noise observed at the receivers. We propose to add the following improvements of the TDGF method: 1) modifications to better handle cases having non-isotropic noise; 2) implementing a system identification approach for obtaining reliable amplitude information for the TDGF, allowing for the estimation of attenuation along paths between receivers. We also seek turning body-wave noise into relative arrival times, and thus improvements of traditional body-wave tomography.

RESEARCH ACCOMPLISHED

Estimating Site Amplification Factors from Ambient Noise

This part is based on Taylor et al. (2009). Most studies of ambient noise have focused on the measurement of interstation group velocities using the time-domain Green's function derived from noise cross correlation (e.g., Gerstoft et al., 2006a). Little work to date has addressed the issue of obtaining attenuation from ambient noise. Recent work of Snieder (2007), Matzel (2008), Prieto and Beroza (2008) and Prieto et al., (2009) have begun to address this problem. Snieder (2007) shows that, for acoustic waves in homogeneous anelastic media, correlation-type Green's functions can be correctly estimated, but attenuation is not. In practical applications, however, multiple scattering may aid in recovering attenuation, but the issue remains unresolved. Snieder (2007) also points out the necessity of dividing observed power spectrum by that of the excitation (forcing) power spectrum that we use in our approach. Ambient noise has been used previously for estimating site effects (e.g., Field and Jacob, 1995) by taking the horizontal to vertical spectral ratio to obtain the resonant frequency. The motivation for our work is related to nuclear explosion monitoring, but may have other applications as well, particularly for seismic hazard studies, calibration of regional arrays and site selection for planned station installations.

We have developed a simple methodology for estimation of site amplification factors (and possibly relative attenuation) using ambient noise. The approach is to estimate site *Q* using standing waves as opposed to taking a propagating wave, tomographic approach (e.g. Matzel, 2008) or the spatial coherency (SPAC) approach of Aki (1957; e.g. Prieto et al., 2009). The idea is to treat time-varying frequency-wavenumber (FK) beams of the ambient noise field as a forcing function beneath a network of stations. Each station responds differently to the forcing function depending on the site structure and attenuation. Differential equations representing different forced, damped harmonic oscillator systems (FDHMO) can be used to estimate *Q* and resonance frequencies beneath stations. Additionally, the method does not rely on any time-domain normalization such as 1-bit normalization (e.g., Benson et al., 2007) that presumably will have a deleterious effect on amplitude measurements necessary for attenuation estimation.

For our analysis, we collected data for the month of January 2008 from the Southern California Earthquake Data Center (SCEDC) for 72 stations shown in Figure 1a. Stations CHF and BRE are examples of a hard rock and soft rock site, respectively, that will be discussed in subsequent analyses. Data for each station was examined for glitches, dropouts or other irregularities that may make them unsuitable for analysis.

Imagine that stations in a network or array are driven by a forcing function derived from the ambient noise field. Each site will respond differently depending upon the elastic and anelastic properties of the underlying medium. As a simple illustration, we use the differential equation for a FDHMO to simulate the response of each station to the forcing function given by (e.g., Lay and Wallace, 1995)

$$\ddot{x} + \gamma\dot{x} + \omega_0^2 x = \frac{1}{M} F(t) \qquad (1)$$

where $F(t)$ is the forcing function, x is the sensor displacement response to the forcing function, γ is the viscous damping term and ω_0 is the natural frequency of the oscillator and M is the mass. For light damping, $\gamma << \omega_0$, the resonance peak is narrow and most of the energy is concentrated around $\omega \approx \omega_0$. Using the approximation $(\omega_0 + \omega)(\omega_0 - \omega) \approx 2\omega_0(\omega_0 - \omega)$ the power spectrum for a particular site relative to that of the forcing function is then given by

$$P_{xF}(\omega) = \frac{P_x(\omega)}{P_F(\omega)} = \frac{M}{\omega_0^2\left[4(\omega_0 - \omega)^2 + \left(\frac{\omega}{Q}\right)^2\right]} \quad (2)$$

where $\gamma = \omega_0/Q$. We leave the mass, M, in the formulation because it will subsequently be related through our observations to the density at each receiver site. Note that the resonant frequency is given by $\omega_0 = \sqrt{(k/M)}$ where k is the spring constant. For each station, it is then possible to grid search over a range of ω_0 and Q values to match the observed resonance peaks. Of course, the single oscillator FDHMO is a very simple system and, as will be seen below, observations suggest that a more complicated representation possibly involving slight nonlinearity may be required.

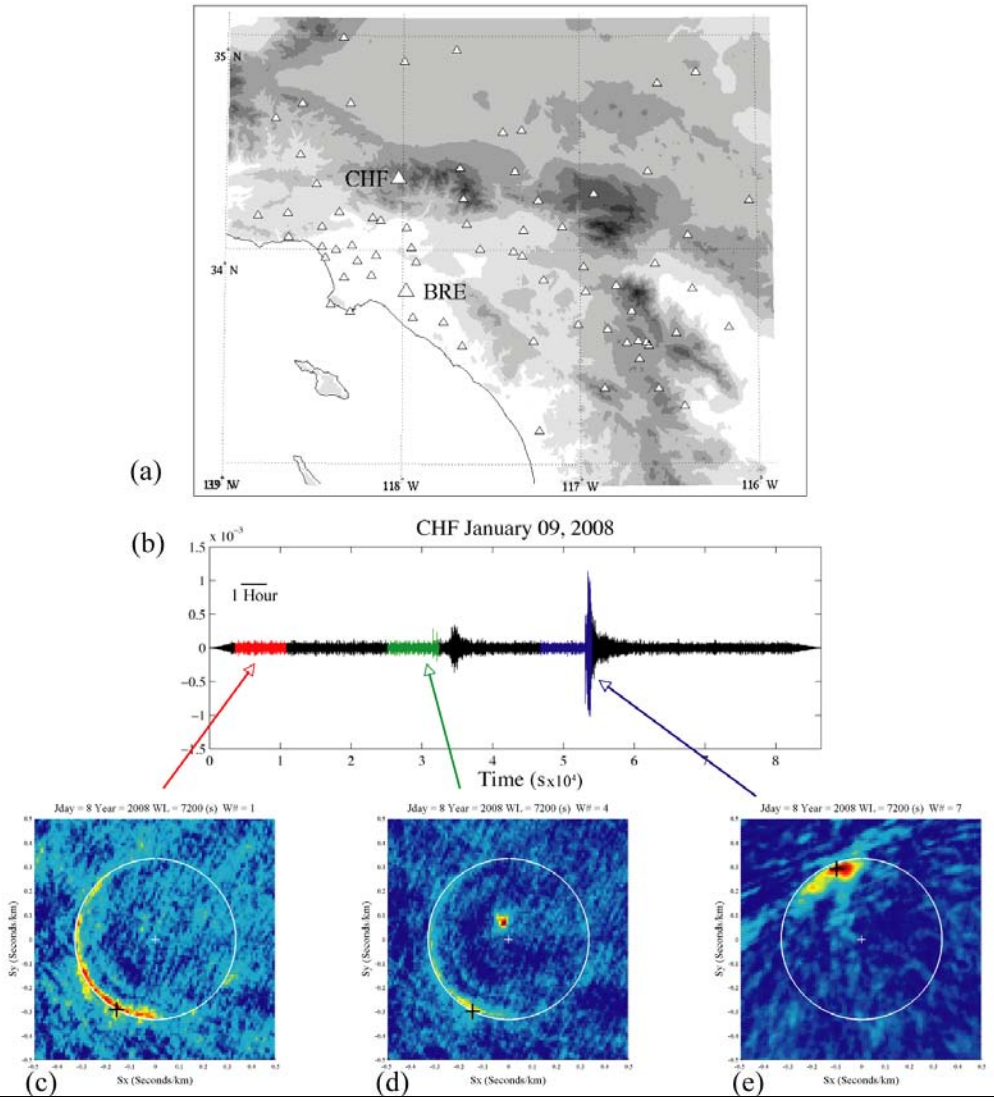

Figure 1. (a) Map showing seismic stations of the SCEDC used in this study. CHF and BRE are examples of hard rock and soft rock sites, respectively. (b) One day of BHZ channel data at station CHF for January 9, 2008. Bottom portion of figure shows FK beams for three 2-hour samples of noise each with a color-coded arrow indicating the portion of the signal used to compute the beam. White circle corresponds to a phase velocity of 3 km/s and black + symbol to the point at which beam is computed. Note that all available stations for this day shown in Figure 1a were used to compute the FK spectrum.

The power spectrum of the forcing function, $P_F(\omega)$ in Equation (2) is computed from the network or array beam directed towards the maximum power of the ambient noise field. A network or array beam is necessary for estimating the forcing function. This process is illustrated in Figure 1 where we compute the FK spectrum between 0.03 and 0.25 Hz. Figure 1b shows the record at station CHF for January 9, 2008, with three two-hour time windows indicated by red, green and blue. Note that all available stations for this day shown in Figure 1a were used to compute the FK spectrum. Three examples of FK spectra are shown color-coded to time windows on the seismogram in Figure 1b. We compute a beam at the point marked by a + symbol for the maximum power between phase velocities of 2.9 and 3.2 km/s.

The FK spectrum in Figure 1c is typical for a noise sample uncontaminated by signal transients. Figure 1d is contaminated by the arrival of a teleseismic *P* wave from the northwest at a high phase velocity although the noise arrivals at relatively lower power can still be seen arriving from the southwest. Restriction of the phase velocities to those between 2.9 and 3.2 km/s allows us to remove the power from the transient *P* wave. Figure 1e shows the FK spectrum for a time window that was excluded from our analysis. A large regional surface wave arrives from the northwest at phase velocities similar to ambient noise. It is a simple matter to identify this and eliminate this time window from the analysis. For the month of January, the noise field arrives predominantly from the southwest although a range of azimuths can be observed consistent with Gerstoft and Tanimoto (2007). In practice, a greater sampling of azimuths will help stabilize results and reduce potential directionally-dependent interference effects on the wavefield from multiple sources and lateral heterogenity. This can be achieved in two ways. The first is by obtaining noise samples over different times of the year. The second is by integrating the FK beam along a semi-circle of azimuth and phase velocity to capture a wider range of ambient noise energy.

Figure 2 shows the processing steps involved with obtaining a site amplification factor from ambient noise for January 9, 2008 shown in Figure 1. We divide the data into two-hour non-overlapping time windows. Figure 2a shows the CHF BHZ power spectrum for each of the noise samples shown in Figure 1b. The power spectrum is computed from each of the broadband FK beam points using the full array and is shown in Figure 2b. Treating the beam power in Figure 2b as the network forcing function and the individual channel power as the response (Figure 2a), we use the center portion of Equation (3) and estimate the site response by computing the power spectral ratio shown in Figure 2c. In our analysis below, we compute the median of the power spectra for each two-hour time segment over all samples passing QC for the month of January 2008 at each station. Note that in our figures the spectral smoothing is only for illustration purposes and not actually performed until the final processing step.

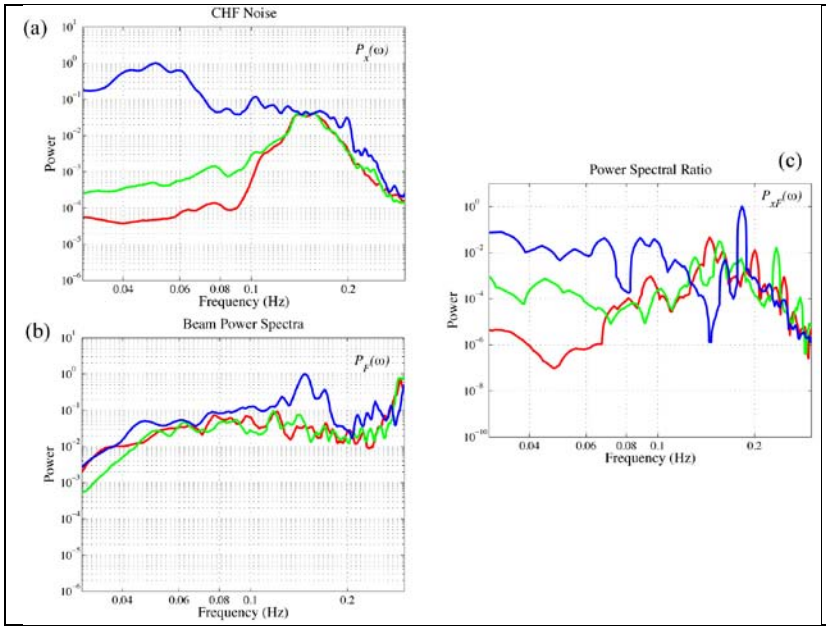

Figure 2. (a) CHF single-channel power spectra from noise taken from each of the three windows of Figure 1b using the same color-coding for station CHF as in Figure 1 for the January 9, 2008 noise sample. (b) Smoothed power spectrum for each of the FK beam points shown in Figure 1. (c) Ratio of CHF noise power (Figure 2a) relative to beam power (Figure 2b).

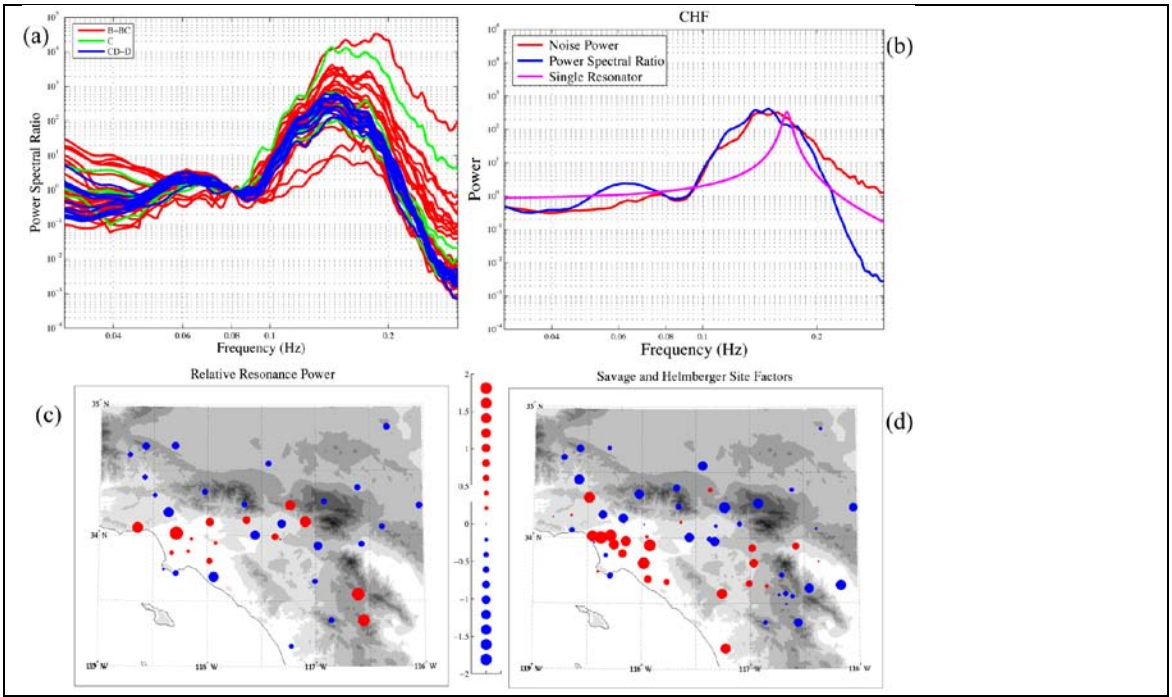

Figure 3. (a) **Individual power spectral ratio median for all stations with NEHRP site classification factors in three groups all normalized at 0.08 Hz. (b) Station CHF smoothed noise power (red) for sample shown in Figure 2a, power spectral ratio median (blue) and single resonance peak (magenta). (c) Map showing standardized relative resonance power. (d) Standardized logarithm of site amplification terms from Savage and Helmberger (2004). In both (c) and (d) red indicates larger amplitudes and blue lower amplitudes. Size of symbol is proportional to absolute value of measurement. Frequency axis in (a) and (b) is between 0.03 and 0.3 Hz.**

A number of features are observed in Figure 2. Most notably is the contamination of the third time window by the large regional event arriving from the northwest (as indicated by the FK plot in Figure 1e). The individual channel is strongly affected by this event as well as the power spectral ratio justifying the elimination of this window from subsequent analysis. In contrast, beamforming on the maximum noise power for the second time window effectively removes contamination of the small teleseismic event arriving from the northwest. The beam power shows a different spectral character than that of the individual channel noise. The individual channel noise spectra show a prominent spectral peak at approximately 0.167 Hz as expected for the microseismic noise peak. In contrast, the beam is flatter and has a subsidiary peak at about 0.3 Hz. A histogram of station spacing indicates that spatial aliasing effects for surface waves propagating at 3 km/s may start to occur at frequencies around 0.3 Hz. Thus, our subsequent analysis focuses on frequencies less than 0.3 Hz.

Figure 3a shows individual station power spectral ratio medians (all normalized at 0.08 Hz) grouped by National Earthquake Hazard Reduction Program (NEHRP) site classifications of Yong et al., (2008). Group B-BC represent soft rock sites, C intermediate, and CD-D hard rock sites. All stations show the same general character with a spectral peak between 0.14 and 0.16 Hz. The hard rock sites (blue) show similar power spectral ratios. In contrast, the soft rock sites show significant variability and there is a tendency for spectral medians to shift to higher frequencies and become broader as the amplitude increases. This could be due either lower density materials at higher amplification sites shifting the resonance frequency to larger values or to slight small-strain nonlinearity for stations having high site amplification (e.g. Assimaki et al., 2008). Figure 3b shows station CHF smoothed noise power (red) for the noise sample shown in Figure 2c, the power spectral ratio median for January 2008 (blue) and single resonance peak (magenta) computed using Equation (3) with a Q of 20 and resonance frequency of 0.167 Hz. The shape of the observed spectrum is similar to that of the microseismic noise except that it is narrower and shifted to slightly lower frequencies. This effect is observed for the other stations as well. This suggests that the power spectral peak is indeed a resonance peak driven by microseisms. Obviously, a single resonator model is not the

correct representation but has the general character of the observed resonance peak in that the lower frequency power level (where the forcing function and site response are in phase) is greater than that of the high frequency power level (where the forcing function and site response are phase shifted by 180°). More complicated attenuation representations (such as absorption band models) will be required to model the nature of the observed resonance peaks (e.g., Liu et al., 1976).

We compute relative resonance power is by taking the average of the logarithm of each station power spectral ratios shown in Figure 3a to that of the median for all stations between 0.08 and 0.3 Hz. Figure 3c shows a map of the standardized resonance power, $Z = (X - \mu_X)/\sigma_X$, (where X is the logarithm of the relative resonance power) and Figure 3d the standardized site amplification terms from Savage and Helmberger (2004) who used the *Pnl* ratio of vertical to radial energy. In general, there is a good comparison between the relative amplitudes of the observed resonance power and the Savage and Helmberger site factors with larger amplitudes in the basin regions and lower amplitudes in the mountainous terrain. Two stations showing large resonance power located at approximately 33.5º N and 116.5º W correspond to low velocities observed along the San Jacinto fault zone (Hong and Menke, 2006).

Local High-Frequency *P* Waves at the Parkfield Array

This part is based on Zhang et al (2009). We analyze vertical-component noise recorded at the Parkfield small-aperture array in California (Figure 4a, ~11 km aperture, mid-January to mid-February 2002) using similar beamforming as in the previous section. Slowness-azimuth spectra from 1-hour noise windows (Figure 9b) shows that most 0.6–2 Hz noise energy at Parkfield comes from the coastal direction at a horizontal slowness of ~0.2 s/km, i.e., a velocity of ~5 km/s. We calibrate the beamformer output using earthquakes with known locations in order to provide reference points for tracking the noise sources. The *P* wave of a coastal earthquake (July 13, 2002; M_L 1.8; 66 km SW of the Parkfield array) shows a slowness of ~0.2 s/km (Figure 9c), implying that the source of the *P*-wave noise is located at a similar distance from the array, i.e., offshore.

The power of the high-frequency *P*-wave noise (1–1.3 Hz) strongly correlates with the offshore wind speed (Figure 5), unlike microseisms that have been found correlating with significant wave heights. We calculated the cross-corrrelation of the beamformed *P*-wave noise power with the wind speed obtained at 8 Pacific sites and 4 land sites. The wind speeds at Pacific sites have indeed similar variations. However, Figure 5a shows that the correlation rises to its highest (CC=0.88) at an offshore site (red square) at azimuth 248º, in agreement with the direction of the noise observed from beamforming (225–270º). In contrast, the correlation is poor at all land sites. The time series of the *P*-wave noise power and the wind speed at the best-correlated site is shown in Figure 5b. Assuming a linear relation, the noise power varies with wind speed at a rate of ~1 dB per m/s.

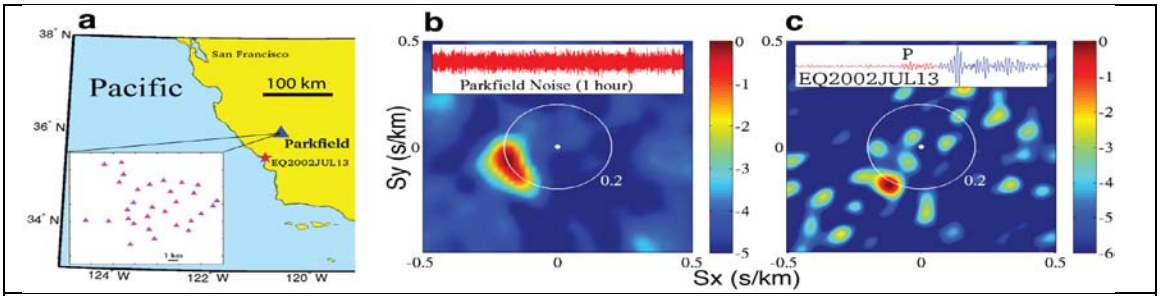

Figure 4. *P*-wave seismic noise observed from beamforming. (a), Map of the Parkfield and one earthquake (red star) for comparison with noise observations. Slowness-azimuth spectra (dB) at 0.7–1.6 Hz are shown for (b) noise and (c) *P*-wave part of a coastal earthquake (July 13, 2002). Waveforms of the noise and earthquakes are shown in the inserts.

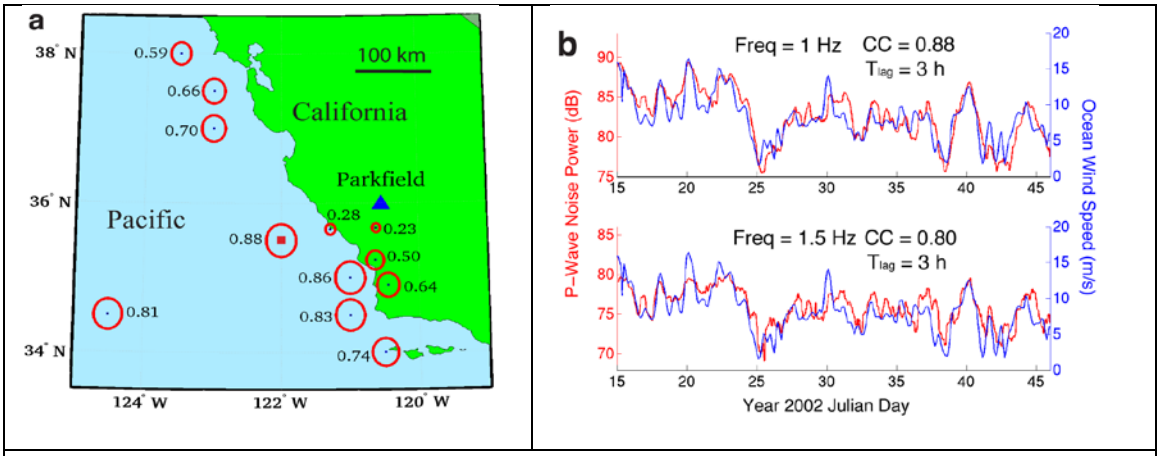

Figure 5. Correlation of the Parkfield *P*-wave noise power (1.0–1.3 Hz) with wind speeds at offshore and onshore sites. (a), Map view of the sites of the Parkfield array (blue triangle) and the wind stations (red circles). The circle size indicates the correlation-coefficient (CC) at each station as marked beside the circles. (b), Time series of noise power (red, at 1 Hz and 1.5 Hz respectively) and wind speed (blue) for the site (red square in a) with the strongest correlation. T_{lag} is the lag time of the peak correlation.

Relative *P*-Wave Arrival Times from Hurricane Katrina to Southern California

The *P* waves observed in Gerstoft et al. (2006b and 2008b) using the southern California seismic network (SCSN), as well as Zhang et al. (2009), can be used to measure relative *P*-wave arrival times across the array from distant noise sources. These relative times contain information about 3-D seismic velocity anomalies under the array. This suggests that it may be possible to perform tomography for crust and upper-mantle structure using a similar approach to that long used to analyze teleseismic *P* waves from earthquakes (e.g., Aki and Lee, 1976), but with the advantage of obtaining data from additional source regions, i.e., the areas of active storms discussed above. Following VanDecar and Crosson (1990), we have validated the basic approach by obtaining a pattern of *P*-wave arrival-time anomalies beneath southern California observed from Hurricane Katrina as a noise source, which is well correlated with that measured by using a nearby earthquake in the Gulf of Mexico (Figure 6).

Our approach includes cross-correlation measurements of relative delay times between station pairs by taking advantage of coherent *P* waves among microseisms, and optimization of relative arrival-time estimates through an over-determined system of timing residual equations in a least-squares sense, assuming that errors in cross-correlation derived delay times are primarily random in nature. For station pairs with a sufficient signal-to-noise ratio (SNR), we generate a system of equations given by $t_i - t_j = \Delta t_{ij}$, and we add the constraint equation $\sum t_i = 0$ to force the arbitrary mean of the relative arrival times to be zero. This system is expressed as $A \cdot t = \Delta t$, where A is a sparse coefficient matrix, for which the i^{th} and j^{th} columns in a row associated with Δt_{ij} are 1 and -1 respectively, while the other columns are zeros. If we weight the equations to reflect the quality of the observations, we have the linear system of the form $W \cdot A \cdot t = W \cdot \Delta t$, where W is a diagonal matrix to weight each equation based on residuals from previously determined unweighted estimate, $res_{ij} = \Delta t_{ij} - (t_i^{est} - t_j^{est})$. A standard approach to solving the equation system in a least-squares sense is the use of normal equations $t^{est} = (A^T \cdot W \cdot A)^{-1} \cdot A^T \cdot W \cdot \Delta t$ by using either the method of singular value decomposition (SVD) or the conjugate gradient algorithm LSQR of Paige and Saunders (1982).

Based on the beamforming output (Figure 7 a & b, [Gerstoft et al. 2006b]), *P*-wave microseisms from Katrina to southern California can be approximated as a plane wave arriving at the network with an apparent speed of 11.7 km/s. The *P* waves can also be clearly revealed by cross-correlating the vertical-component seismic noise recorded at pairs of stations (Figure 7c). The time lags between traces (Δt_{ij}) at any station pair are then obtained as the offset of the maximum of their cross-correlation functions (red dots in Figure 7c).

We have found that the equation residuals derived from the best-fitting solutions are nearly normally distributed (Figure 8a). To evaluate the reliability of the least-squares estimates of the relative *P* arrival times using seismic noise, we then perform a statistical resampling analysis ("bootstrap" method, Efron, 1982; Shearer, 1997; Waldhauser and Ellsworth, 2000). Figure 8b shows that a level of 0.1 s of timing errors can be reached, which may be sufficient for revealing large travel-time anomalies on the order of 1 s.

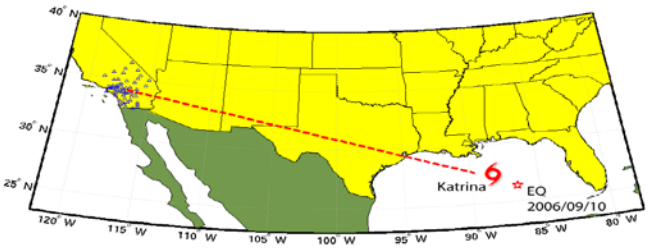

Figure 6. Map of the Southern California Seismic Network, Hurricane Katrina (schematic) on August 28, 2005, and an Mw 5.9 earthquake on September 10, 2006. The dashed line indicates the great circle path (27°) of the *P* waves from Katrina to Southern California.

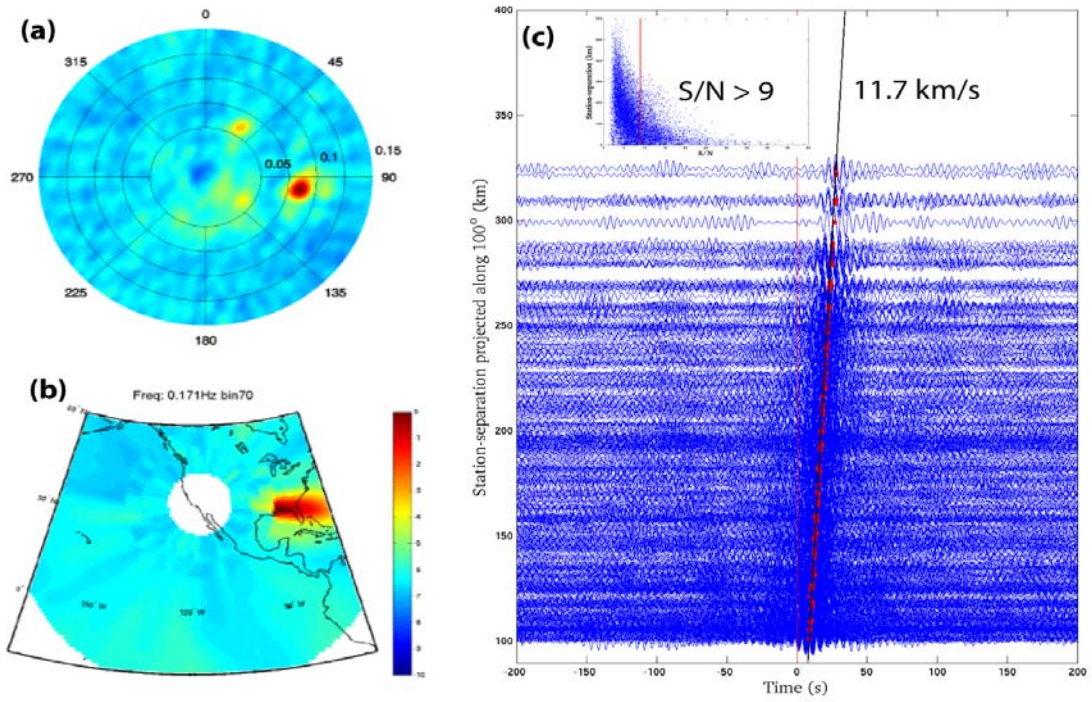

Figure 7. Katrina-generated *P* waves observed in southern California and relative *P* arrival times from cross-correlation. (a) Beamforming of 0.19-Hz vertical-component seismic noise recorded by the Southern California network, showing *P* waves (0.085 s/km, i.e., 11.7 km/s) coming from 100° during Katrina's landing; (b) Source region of *P* waves approximated by back-propagating the slowness-azimuth spectra from (a); (c) Range-time representation of the cross-correlation time series for 400 station pairs with SNR>9. Red dots mark the relative arrival-time measurements as the offset of the cross-correlation maximum. Black line indicates an 11.7 km/s plane wave. The insert shows SNR versus station separation (projected along 100°).

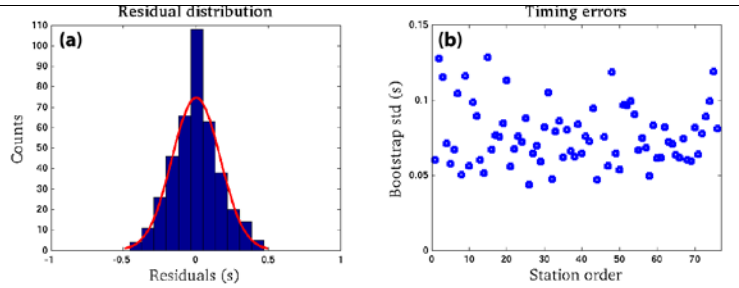

Figure 8. Least squares and uncertainty estimation. (a) Histogram of cross-correlation residuals derived arrival-time lags and least-squares solutions, showing a Gaussian-like distribution. (b) Bootstrap-resampling derived timing uncertainties of the *P* relative arrival times from Katrina noise.

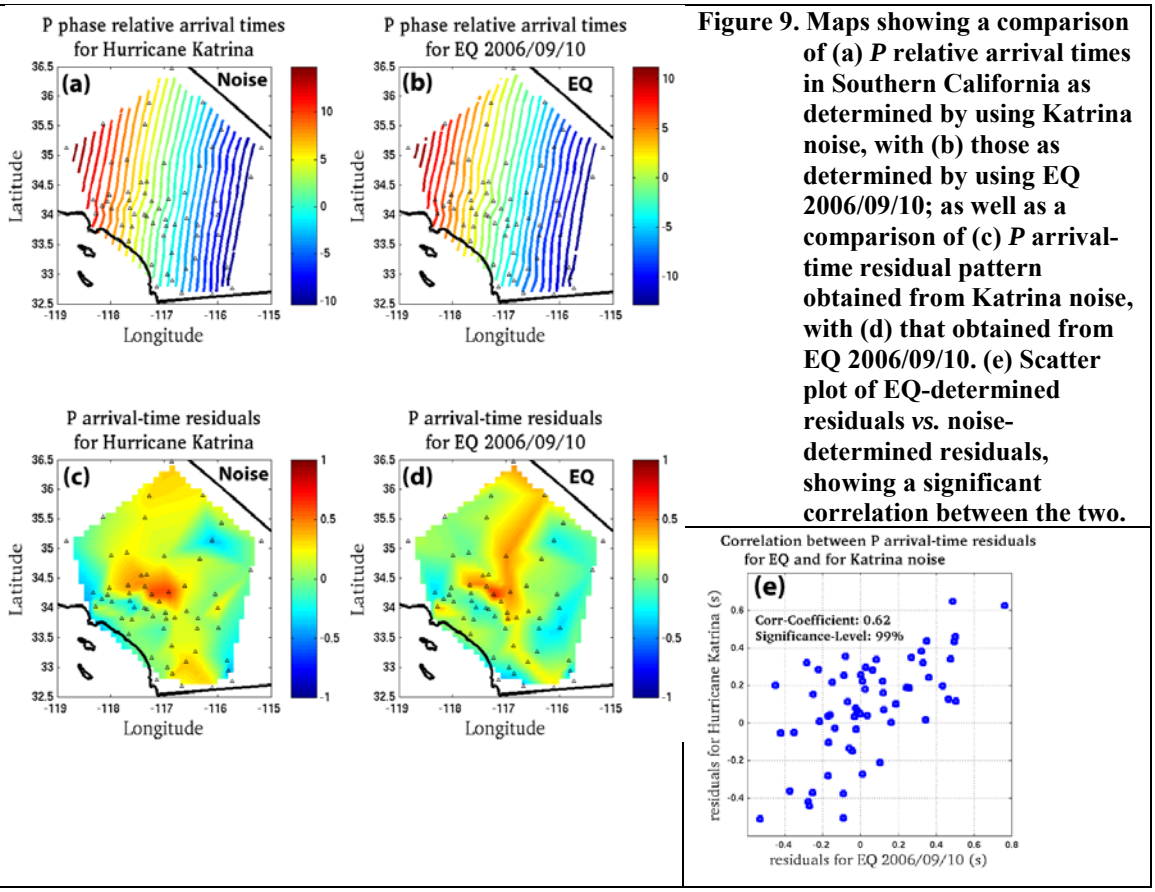

Figure 9. Maps showing a comparison of (a) *P* relative arrival times in Southern California as determined by using Katrina noise, with (b) those as determined by using EQ 2006/09/10; as well as a comparison of (c) *P* arrival-time residual pattern obtained from Katrina noise, with (d) that obtained from EQ 2006/09/10. (e) Scatter plot of EQ-determined residuals *vs.* noise-determined residuals, showing a significant correlation between the two.

To demonstrate this approach, we compare the relative *P* arrival-time estimates by using Katrina microseisms with those estimates through the same processing but by using an Mw 5.9 earthquake that occurred in the Gulf of Mexico on September 10, 2006. The relative *P* arrival times using the earthquake and, thus, their residuals relative to the ak135-predicted times are shown in Figure 9 a & c respectively. Similarly, the estimates using Katrina noise and their residuals relative to an 11.7 km/s plane wave are shown in Figure 9 b & d respectively. It can be seen that the relative arrival times and their anomalies resulting from using *P*-wave microseisms are reasonably well correlated with those resulting from using traditional sources, i.e., earthquakes. To quantify this, the correlation between the two residual patterns is 0.62 with a significance level over 99% (see Figure 9e).

CONCLUSIONS AND RECOMMENDATIONS

1. We have developed a standing-wave methodology that has the potential for estimating frequency-dependent site factors for a network or array of stations using ambient noise. The basic idea behind the method is to use the FK

beam of the ambient noise field to simulate the forcing function beneath the network. Each site will respond differently to the forcing function depending on the local velocity and attenuation structure. The frequency range of applicability is controlled by the spatial aperture and station spacing used to construct the FK beam. Results using a month of ambient noise data in southern California are encouraging in that the shape and amplitude of individual station resonance peaks appear to correlate with local geology and with site factors of Savage and Helmberger (2004). In general, hard rock sites are characterized by lower amplitude, narrower resonance peaks than those from soft rock sites. There is also a tendency for spectral peaks to shift to higher frequencies and become more asymmetric as the amplitude increases. This could be due to lower densities or to small-strain nonlinearity at stations having high site amplification (e.g., Assimaki et al., 2008).

2. A test examining teleseismic *P* waves recorded in southern California shows that similar arrival-time anomalies can be obtained both from direct *P* waves from a natural earthquake and *P*-wave noise generated by a large storm. This suggests using storms as additional sources for relative arrival time measurements.

REFERENCES

Aki, K. (1957). Space and time spectra of stationary stochastic waves, with special reference to microtremors, *Bull. Earthq. Res. Inst.* 35: 415–457.

Aki, K. and W. H. K. Lee (1976). Determination of three-dimensional velocity anomalies under a seismic array using first P arrival times from local earthquakes 1. A homogeneous initial model, *J. Geophys. Res*. 81: 4381–4399.

Assimaki, D., W. L. J. Steidl, and J. Schmedes (2008). Quantifying nonlinearity susceptibility via site-response modeling uncertainty at three sites in the Los Angeles Basin, *Bull. Seismol. Soc. Am*. 98: 2364–2390.

Bensen, G.D., M.H. Ritzwwoller, M.P. Barmin, A.L. Levshin, F. Lin, M.P. Moschetti, N.M. Shapiro and Y. Yang (2007). Processing seismic ambient noise data to obtain reliable broad-band surface wave dispersion measurements, *Geophys. J. Int.* 169: 1239–1260.

Efron, B. (1982). *The jackknife, the bootstrap, and other resampling plans*, SIAM, Stanford University, Philadelphia, 92 pp.

Field, E. H. and K. H. Jacob (1995), A comparison and test of various site-response estimation techniques including three that are not reference-site dependent, *Bull. Seismol. Soc. Am*. 85: 1127–1143.

Gerstoft, P., K. G. Sabra, P. Roux, W.A. Kuperman, and M.C. Fehler (2006a). Green's functions extraction and surface-wave tomography from microseisms in southern California, *Geophys*. 71: SI23–SI31.

Gerstoft, P., M.C. Fehler, and K. G. Sabra (2006b). When Katrina hit California, *Geophys. Res. Lett*. 33: L17308, doi:10.1029/2006GL027270.

Gerstoft, P. and T. Tanimoto (2007). A year of microseisms in southern California, *Geophys. Res. Lett*. 34: L20304, doi:10.1029/2007GL031091.

Gerstoft, P, P Shearer, N Harmon, and J Zhang (2008b). Global P, PP, and PKP wave microseisms observed from distant storms, *Geophys. Res. Lett*. 35: L23307, doi:10.1029/2008GL036111.

Hong, T.K. and W. Menke (2006). Tomographic investigation of the wear along the San Jacinto fault, southern California, Phys. Earth and Planet. Int., 155, 236-248.

Lay, T. and T. Wallace (1995). Modern Global Seismology, Academic Press, San Diego, CA.

Liu, H.P., D.L. Anderson and H. Kanamori (1976). Velocity dispersion due to anelasticity: Implications for seismology and mantle composition, Geophys. J.R. Astron. Soc., 47, 41-58.

Matzel, E.M. (2008). Attenuation tomography using ambient noise correlation, *Seism. Res. Lett*. 79: 358.

Paige, C. C., and M. A. Saunders (1982). LSQR: Sparse linear equations and least squares problems, ACM Transactions on Mathematical Software 8/2, 195–209.

Prieto, G.A. and G.C. Beroza (2008). Earthquake ground motion prediction using the ambient seismic field, *Geophys. Res. Lett*. 35: L14304, doi:10.1029/2008GL034428.

Prieto, G. A., J. F. Lawrence and G. C. Beroza (2009). Anelastic Earth structure from the coherence of the ambient seismic field, accepted by *J. Geophys. Res*.

Savage, B. and D. V. Helmberger (2004). Site response from incident Pnl waves, *Bull. Seismol. Soc. Am*. 94: 357–362.

Shearer, P. (1997). Improving local earthquake locations using the L1 norm and waveform cross correlation: application to the Whittier Narrows, California, after shock sequence, *J. Geophys. Res*. 102: 8269–8283.

Snieder, R. (2007). Extracting the Green's function of attenuating heterogeneous acoustic media from uncorrelated waves, *J. Acoust. Soc. Am*., doi: 10.1121/1.2713673.

Taylor, Steven R., P. Gerstoft, and M. C. Fehler (2009). Estimating site amplification factors from ambient noise, *Geophys. Res. Lett*. 36: L09303, doi:10.1029/2009GL037838.

VanDecar, J. C., and R. S. Crossen (1990). Determination of teleseismic relative phase arrival times using multi-channel cross-correlation and least squares. Bull Seismol Soc Am, 80: 150–169.

Waldhauser, F. and W. L. Ellsworth (2000). A double-difference earthquake location algorithm: method and application to the northern Hayward fault, California, *Bull. Seismol. Soc. Am*. 90: 1353–1368.

Zhang, J., P. Gerstoft, and P. M. Shearer (2009). High-Frequency seismic noise driven by ocean winds, *Geophys. Res. Lett*. 36: L39302, doi:10.1029/2009GL037761.